Electronic Supplementary Information (ESI)

S1 - QY System

Fig. S1 shows a simplified sketch of the QY system built in the lab to perform the characterisation of the UCNPs. A magnification of the top view of the region of interest (ROI) is highlighted in the top right corner of the figure. The details of the optical components are summarised in the Table S1. The calibration of the system was made by replacing the 976 nm laser with a 785 nm laser to excite the reference dye (DY-781-01 purchased from Dyomics GmbH), which was placed in a cuvette in the sample holder. The short pass optical filter SP was replaced by a long pass LP in order to filter the 785 nm laser light from the 800 nm emission of the dye DY-781-01. The mirrors FM were flipped down for BP1 illumination and flipped up for BP2 illumination.

L= Lens; P= Polarizer; FM = Flip mirror; M = Mirror; I = Iris diaphragm; PM = Power meter; S = Slit; BP = Bandpass filter; SP = Shortpass filter; ND = Neutral density filter; BS = Beamsplitter;
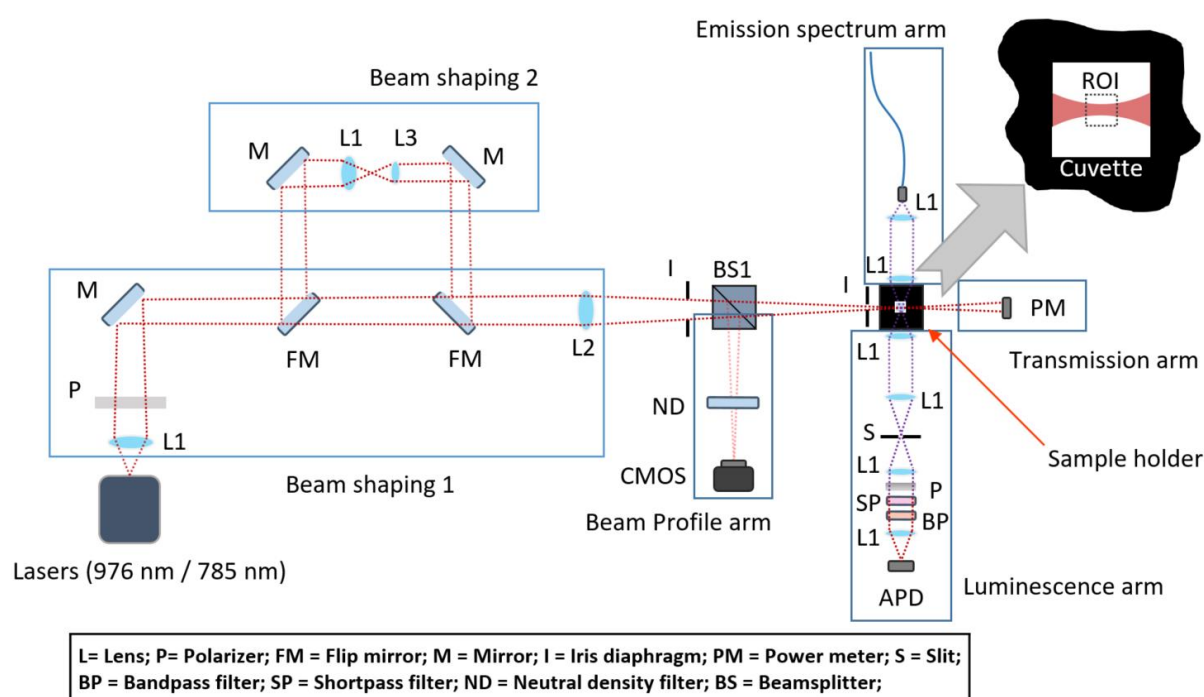
Fig. S1: Quantum Yield system for relative measurements including beam profile compensation.

Table S1: Specification of the components used on the QY system on the QY system.

Components	Specification
L1	Lens: focal length 30 mm
L2	Lens: focal length 200 mm
L3	Lens: focal length 8 mm
P1	Polarizer at 0° (vertical alignment)
P2	Polarizer at 54.7° (Magic angle)
BS	Beam splitter 98:2
ND	Variable neutral density filter (OD: 3 or 4)
S	Slit: 1 mm aperture
SP	900nm short pass filter: Thorlabs - FESH0900 (For UC)
LP	785 nm Long pass filter: Semrock - LP02-785RE-25 (For the reference Dye)
BP	800 nm Band pass filter: Thorlabs - FEBH800-40 band width 40 nm

S2 - Absorption coefficient evaluation

When light crosses the cuvette containing UCNPs diluted in water, its total attenuation coefficient (μ coefficient shown in equation S1) is given by the contribution due to water and cuvette (together represented by the μ_b coefficient), scattering (represented by μ_s), and the UCNPs absorption (μ_a).

$$\mu = \mu_a + \mu_s + \mu_b \qquad S1$$

To determine μ_a, first μ and μ_b were obtained at the 976 nm wavelength for various power densities covering the low beam power density range (obtained with BP2) and the high beam power density range (obtained with BP1). Immediately after this narrow band measurement, a broad band white light measurement was conducted to determine μ_s, which details are explained in the next section.

A quartz cuvette was filled with distilled water to determine μ_b and another identical cuvette was filled with the UCNPs solution to determine μ according to equation S2, which gives the light attenuation through a media according to the Lambert's law,

$$\mu . l = \ln \frac{P_o}{T} \qquad S2$$

where, l is path length of the light crossing the media, which is equal to 1 cm (length of the cuvette), P_o represents the incident power (or laser power), and T represents the transmitted power. Both, P_o and T were measured with power meter and to increase the signal to noise ratio, 600 data points were averaged for each laser power. The results and the associated errors are shown in figure S2.
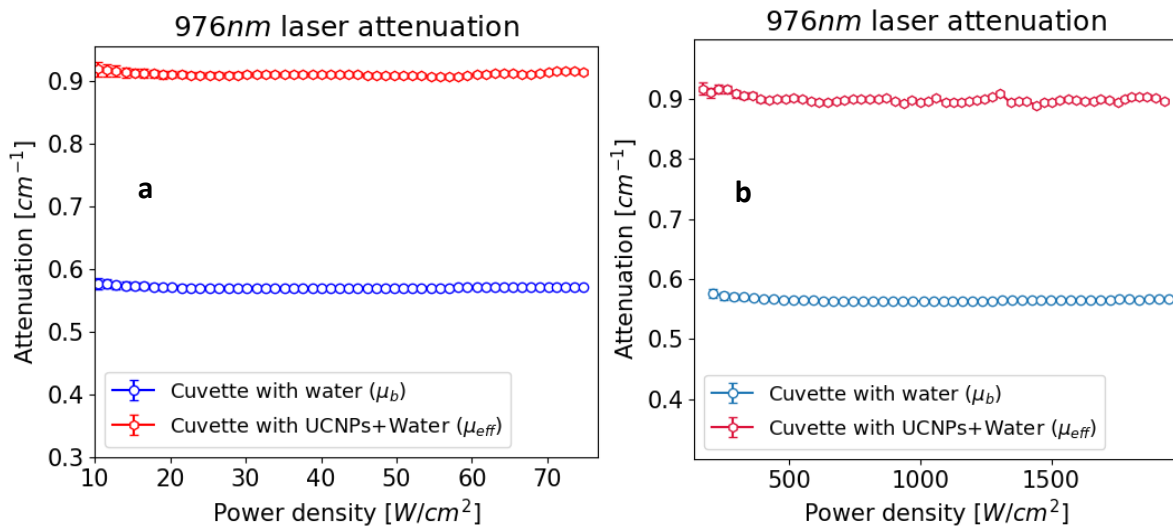
Figure S2: Attenuation coefficient for the 976 nm laser light crossing a quartz cuvette containing UNCPs dispersed in water (top curves in red), μ, or distilled water (bottom curves in blue), μ_b. a) Low beam power density obtained with BP2 and b) high beam power density obtained with BP1. The associated errors are plotted as error bars in both plots.

The fluctuations observed for μ are due to the movement of small UCNP clusters in the liquid solution. Apart from this effect, the UCNPs' effective attenuation behaves as a constant for the entire studied beam power density range. Therefore, subtracting the distilled water attenuation from the

UCNPs+Water, the attenuation due to the UCNPs alone represents the absorption and scattering contributions, $\mu_a + \mu_s$. The averaged value for the attenuation at 976 nm was plotted in figure S3.a.

S3 - Accounting for the scattering contribution

To obtain the scattering contribution, the same experiment as described above was repeated replacing the 976 nm laser with a broadband white light source and acquiring the transmitted spectrum through the cuvettes with the spectrometer instead of the power meter. The wavelength dependent attenuation for the UCNPs alone (*i.e.* already accounting for μ_b) is shown in the figures S3.a by the continuous line. Apart from the peak at 976 nm (due to absorption), the attenuation along the entire wavelength range is due to scattering, which can be approximated by a power law function, equation S3,

$$\mu_S = \mu_o \left(\frac{\lambda}{\lambda_o}\right)^b \ (S3)$$

where, μ_s is the scattering coefficient as a function of wavelength λ, μ_o represents the scattering coefficient at the normalisation wavelength λ_o, and b is a parameter related to the particles size. Therefore, fitting the interval (800 nm to 930 nm) of the broadband data and extrapolating the curve until 1100 nm, the scattering at the excitation wavelength (976 nm) and at the emission wavelength were determined and shown in figure S3.a by the dashed line.
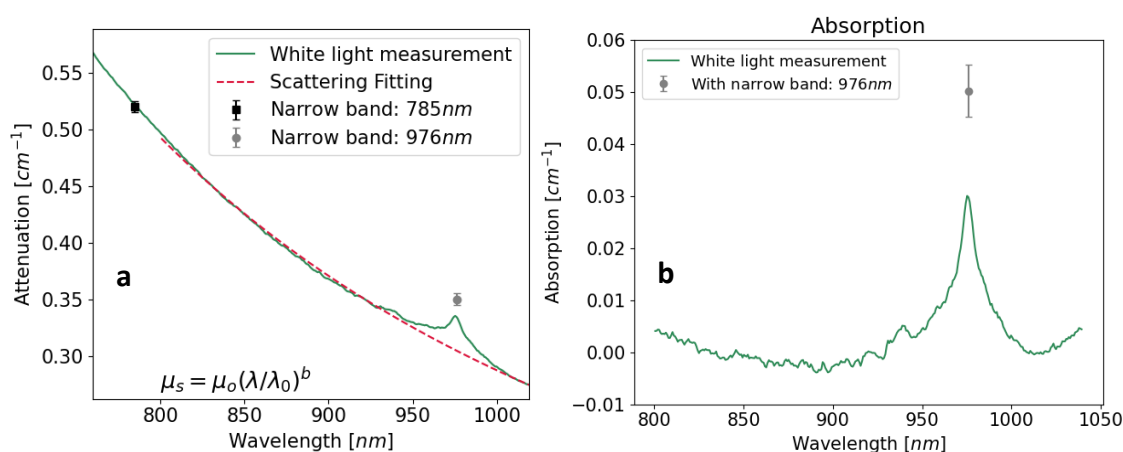
Figure S3: a) Broad band attenuation of UCNPs (continuous green line) along with narrow band measurements (square and circle). Red dashed line represents the scattering contribution obtained from the fitting with equation S3. b) Absorption coefficient obtained from the subtraction of the scattering contribution.

Comparing the attenuation peak from the broadband measurement with the attenuation obtained from the 976 nm narrow band measurement (grey circle in figure S3), one can notice that both peaks do not coincide. The reason for this is that the spectrometer does not have sufficient spectral resolution to resolve fully this narrow absorption peak, which might result in a wider and lower intensity peak. To investigate this effect further, the narrow band experiment was repeated at a different wavelength away from the absorption peak - 785 nm. This was conducted immediately after the broadband white light measurement to ensure the same particle distribution inside the solution without any important change in scattering. The processed 785 nm attenuation coefficient was also plotted in figure S3 (black square), and it precisely overlaps with the broadband measurement. Finally, the scattering contribution was subtracted from the total attenuation giving as a result the curve and the data point shown in figure S3.b. Therefore, the absorption coefficient ($\mu_a =$

$(\mathbf{4.9 \pm 0.4}) \times \mathbf{10^{-2}} \ \mathbf{cm^{-1}})$ was obtained from the narrow band experiment after subtracting the scattering contribution from the broad band one as described above.

S4 – Luminescence spectra
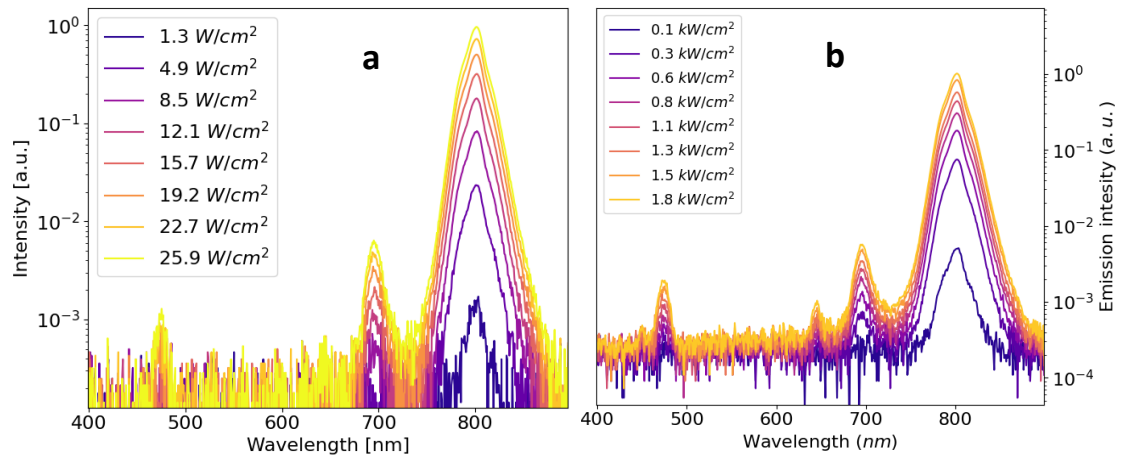
Figure S4: Luminescence spectra of the UCNPs for various power densities in semi-y-log scale. The a) measurement was performed with BP2 and b) with BP1. The Intensity values for each plot were divided by the maximum intensity of the highest peak for normalisation.

S5 – QY evaluation for various definitions on obtaining the excitation power density
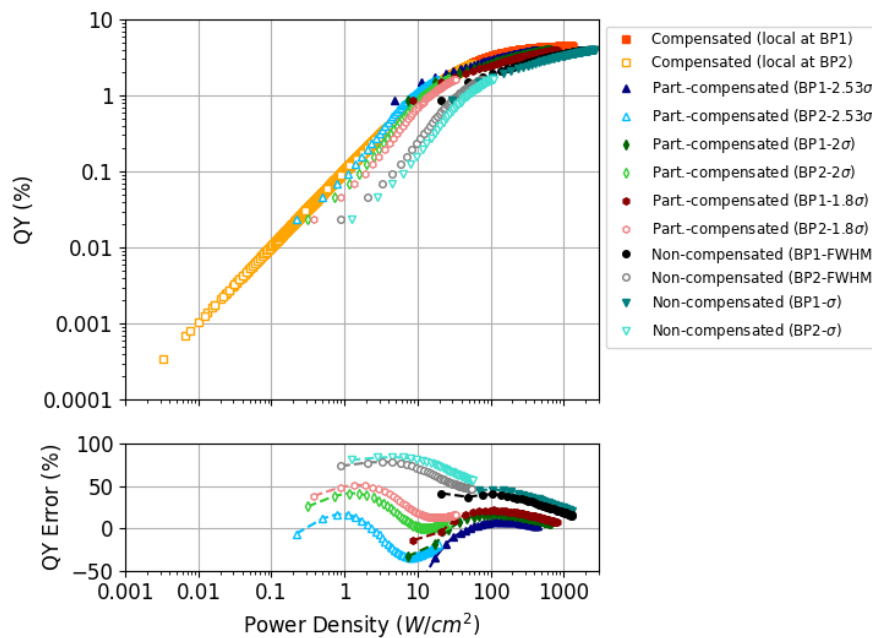
Figure S5: QY versus power densities. Different methods on determining the beam power density is compared to the beam profile compensate iQY (local evaluation – squares).

S6 – The relation between local beam-profile-compensated iQY and non-compensated QY

The wide dynamic ranges of power densities and local iQY were obtained by fitting the luminescence data with the equation 6 (shown in the paper) and simplified here as equation S4,

$$L_r = C \, \eta_b \sum_{k=0}^{N} \frac{\rho_k^2}{\rho_k + \rho_b} \quad (S4)$$

which highlights the local power density at the pixel level ρ_k, the balancing point constants ρ_b and η_b, and combines the product of the other constants as C. The model utilised to determine equation S4, and the quality of the fitting (figure 3) ensured the reliability of the wide dynamic range of the compensated iQY. The same parameters η_b and ρ_b (table 1) are able to represent all the measured resultant data for both curves (from BP1 and BP2), which contains several local power density data points. For each beam profile, 70 L_r data points, each containing more than 30000 ρ_k points (200 unique ρ_k, which overlap at low power densities for the QY data - see figure S6) were used on the fitting process. Notice the large overlap and wide dynamic range of the local evaluation (X markers) in figure S6 obtained with only 4 corresponding L_r data points (Hexagons).
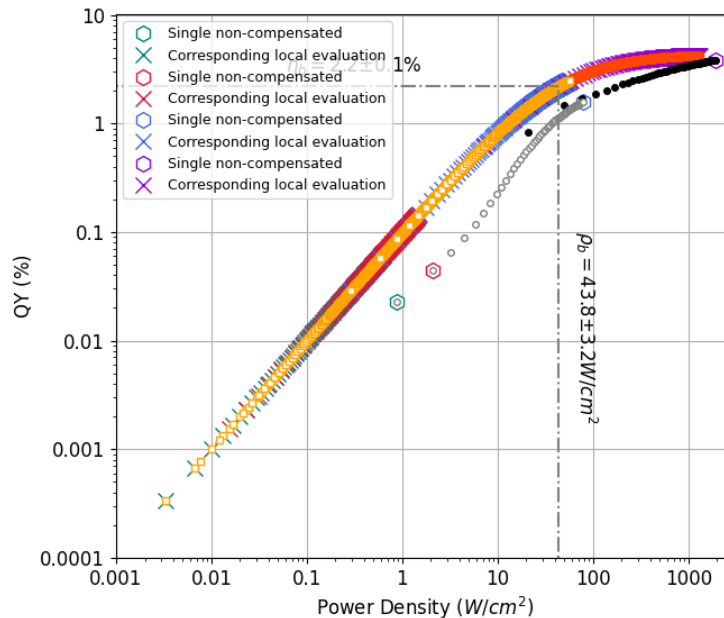
Figure S6: Local beam profile compensated iQY (yellow and orange squares) and non-compensated QY (grey and black circles). Hexagons and X markers represent the relation between a non-compensated QY with its corresponding local evaluation, respectively.